Temperature Behavior During Multistage Fracture Treatments in Horizontal Wells

Xinyang Li and **Ding Zhu,** Texas A&M University

Summary

Downhole temperature measured by distributed-temperature sensors (DTSs) shows distinct response to injection and shut-in during multistage fracture treatments in horizontal wells. A thermal model predicting temperature distribution along the wellbore is essential to use the DTS technology to quantitatively diagnose fracture treatments. With inversion, the model can be used to translate downhole-temperature measurement to downhole flow distribution, and therefore to estimate fracture efficiency.

In this paper, we present a thermal/flow model that predicts temperature distribution in a system that contains reservoir, wellbore, and fractures during fracture propagation and after well shut-in. We coupled a wellbore-flow model with a simple fracture-propagation model to predict fracture half-length and fluid distribution. For a single-stage fracture treatment, a transient wellbore thermal model is coupled with the fracture and formation thermal models, which are derived from the energy-conservation equations. A sequential simulation method is then applied for multistage fracture treatments by considering the treatment schedule. The full model has three modes: no fracture, fracture propagation, and warm back for shut-in. The full model is used to simulate the stage that is under fracturing. Once the fracture pumping is finished, warm back of the entrained fracture fluid during shut-in periods is simulated by removing the convection term and implementing the corresponding boundary conditions. Numerical solutions are necessary for time-dependent fluid loss and complex nonlinear heat exchange. Mass- and energy-conservation equations are solved by use of the fully implicit finite-difference approach for the conjoint gridding system. The results of the fracture and formation model are verified by analytical solutions for simplified cases.

This paper provides synthetic case studies in a low-permeability reservoir by use of the integrated model. The influences of fluid distribution, fluid loss caused by natural and induced fractures, DTS-deployment locations, and reservoir-heat-transfer parameters on temperature behavior are investigated. At the creation and propagation of fractures, injection flow rate (convection) plays an important role on fracture propagation and leakoff front movements. Heat conduction is the dominant mechanism governing temperature response during shut-in. By use of the algorithm for single-stage treatment, a work flow for multistage fracture simulation is created by performing a single-stage stimulation, shutting in the stage, and moving to the next stage along the wellbore. For a shale reservoir, the time frame to reach thermal equilibrium is on the order of weeks, and this gives the possibility to identify the flow-rate distribution from temperature measurements. Sensitivity of fluid distribution, fluid loss, DTS fiber-cable locations for different completion methods, and reservoir parameters is examined, which helps us to understand temperature behavior for fracture diagnosis by use of DTS data during stimulation operations.

The methodology developed in this work can be a complementary component to a model that predicts temperature behavior during production to provide better boundary conditions, and it can also be a standalone tool to analyze fracturing-fluid distribution.

Introduction

Multistage hydraulic fracturing has offered one of the best solutions to develop complex unconventional oil and gas reservoirs, which requires multiple-stage hydraulic fracturing in horizontal wells. Monitoring and diagnosis of fracture treatment is a critical step to the success of fracture stimulation.

Recently, fiber-optic DTS has been widely used as a tool for fracture monitoring. This technology not only offers continuous real-time monitoring for the entire wellbore, which enables one to observe dynamic temperature profiles during multistage fracture treatments, but it is also more affordable compared with fracture-mapping techniques by microseismic. It has brought the information from temperature data to allow the estimation of fracture-creation depth, vertical coverage, number of generated fractures, effects of diverting agents, and undesired flow behind casing (Sierra et al. 2008). Holley et al. (2012) also stated that the DTS offers real-time monitoring for identifying, quantifying, and evaluating near-wellbore fracture geometry, fracturing-fluid distribution, and overall stimulation effectiveness. In the study, Holley et al. (2012) coupled fracture-treatment responses and openhole-log characteristics with the near-wellbore DTS data during pumping and warm back to perform an integrated assessment of the completion-stimulation effectiveness and efficiency. Compared with production-logging tools, DTS is more flexible and can be used for both short-term and long-term scenarios (Johnson et al. 2006). Sierra et al. (2008) and Huckabee (2009) used DTS data for field cases to diagnose hydraulic-fracture stimulation and evaluate well performance. Molenaar et al. (2012) presented different horizontal-well cases to illustrate how the combination of DTS and distributed-acoustic sensing has the potential to enhance the monitoring, assessment, and optimization of hydraulic-fracture-stimulation treatments with openhole completion and limited-entry-perforation completion. Ugueto et al. (2014) evaluated the efficiency of the hydraulic-fracture-simulation treatments by use of DTS data, considering both near-wellbore and far-field diagnostics. Later, Ugueto et al. (2015) reviewed examples from multiple wells where fiber optics were used to gain a better understanding of three fracture-simulation topics: diversion, stage isolation, and overflushing.

To interpret temperature measurements, theoretical models are needed. One of the earliest temperature models presented by Ramey (1962) predicted temperature profiles as a function of time and depth for vertical single-phase-flow wells. Hagoort (2004) improved the Ramey (1962) model and provided solutions by eliminating the assumption of neglecting heat accumulation in that work. Hasan and Kabir (1991) contributed to the wellbore thermal model by proposing early-time transient temperature behavior of fluid flow in the wellbore and adopting appropriate boundary conditions between the formation and the wellbore. They also applied the superposition principle to account for the gradual changes in heat-transfer rate between the wellbore and the formation with respect to time. Yoshioka

This paper (SPE 181876) was accepted for presentation at the SPE Asia Pacific Hydraulic Fracturing Conference, Beijing, 24–26 August 2016, and revised for publication. Original manuscript received for review 23 July 2016. Revised manuscript received for review 13 March 2017. Paper peer approved 16 March 2017.

et al. (2007) proposed methods to interpret measurements for complex wells by use of downhole-pressure and temperature-sensor data. In Yoshioka et al. (2007), a steady-state wellbore thermal model was developed for a horizontal well coupled with a reservoir thermal model. Ouyang and Belanger (2006) developed a numerical model to obtain single-phase-flow profile in horizontal wells by use of downhole measurements. Li and Zhu (2010) established a forward model for wellbore- and reservoir-temperature simulation by use of downhole pressure and temperature data to solve for flow profile in a horizontal well. The Yoshioka et al. (2007) wellbore model was applied and combined with a 3D multiphase reservoir thermal model in the Li and Zhu (2010) work. Hoang et al. (2011) proposed a model for interpreting DTS data during hydraulic fracturing in a vertical well with limited entry and constant fracture geometry. Tabatabaei and Zhu (2011) presented a thermal model to simulate temperature distribution during injection and shut-in of a horizontal well with multiple fractures that have fixed geometries.

In addition to steady-state wellbore thermal models, Maubeuge et al. (1994a, 1994b) developed a numerical thermal model for the reservoir to solve for transient temperature profile that considers small thermal effects, such as the Joule-Thomson effect and viscous dissipation. Duru and Horne (2008) and Sui (2009) proposed transient wellbore thermal models, as well as transient reservoir thermal models. Bahonar et al. (2010) presented a numerical nonisothermal two-phase-flow wellbore simulator coupled with tubular and cement material, and surrounding formation. Bahonar et al. (2010) compared this model with other five models for formation-temperature simulation. With validation against field data, Bahonar et al. (2010) showed the model's merits in predicting casing temperature.

Fracture temperature is also studied by many researchers. Kamphuis et al. (1993) developed a temperature model in the fracture by calculating the heat transfer between the fracture and the formation. Meyer (1989) proposed analytical solutions of thermal models in PKN (Perkins-Kern-Nordgren) and KGD (Khristianovic-Geertsma-de Klerk) fractures coupled with 2D fracturing-fluid flow. Schechter (1992) showed a less-rigorous approach to readily solve the temperature distribution for various fracture geometries, such as 1D propagation of rectangular and penny-shaped fractures. Schechter (1992) considered constant injection-fluid temperature and reservoir initial temperature as boundary conditions, as well as constant fracture width. Seth et al. (2010) developed a fracture thermal model for interpreting DTS data near perforation locations for a single fracture in vertical wells during fracture propagation and after shut-in of the well. Recently, Amini et al. (2015) presented a 3D hydraulic-fracture thermal model to determine temperature profiles in and around the fracture by use of a pseudo-3D fracture-propagation model. On the basis of the simulated results, they concluded that the location of the optical-fiber cable is very important in DTS temperature measurement. Sierra et al. (2008) also noted an analysis of the effect of fiber-optic locations on the temperature response by use of DTS data in hydraulic fracturing.

In this study, wellbore, fracture, and reservoir thermal models are fully coupled with a simple fracture-propagation model to study transient temperature behavior in real time during multistage fracture treatments in horizontal wells. Comparisons with analytical solutions under specific assumptions are also performed by use of the fracture and reservoir thermal model. By use of the coupled thermal model, we are able to simulate temperature distribution to identify fracture locations, estimate flow-rate distribution, and evaluate effectiveness of zonal isolation.

Integrated Forward Model

The forward model consists of a wellbore model, a fracture model, and a reservoir model, and **Fig. 1** shows the schematic of the system used to develop the model. The wellbore- and fracture-flow models are built by use of the mass-conservation equation. Three thermal models are formulated by use of the energy conservation of the defined domain, and solved simultaneously with proper boundary conditions at the perforation location and the fracture/formation interface during injection and after shut-in, respectively. The single-phase wellbore-flow model developed by Yoshioka et al. (2007) and the transient wellbore thermal model presented by Sui (2009) are adopted and modified for well injection in particular. For multistage fracture treatments, the wellbore model is coupled with the fracture and reservoir model sequentially for each stage because of the stage isolation. The mass- and energy-balance equations are presented.

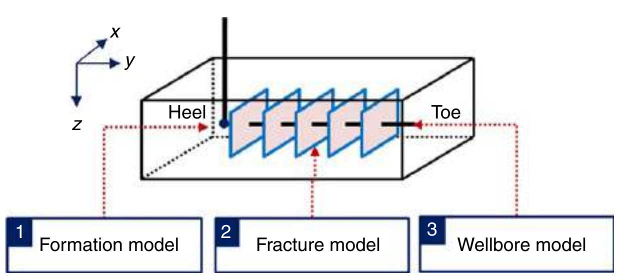

Fig. 1—Schematic of the forward model.

There are three linear-flow regimes in the modeled domain: the flow along the wellbore, the flow along the fracture during fracture propagation, and the leakoff to the formation. The fracturing-fluid-flow directions during injection of a single fracture system in 2D Cartesian coordinates are shown in **Fig. 2.** The problem is modeled for the entire domain and solved more than one-quarter of the domain because of the symmetric nature. During injection, all three flows exist, bringing in heat-convection terms to the thermal equations. During warm back after shut-in, only heat-conduction terms remain in the thermal equations.

Mass-Conservation Equations. The modified wellbore continuity equation during the injection period is

$$\frac{\partial \rho_I}{\partial t} = \frac{2\gamma}{R}\rho_I v_I - \frac{\partial \rho_I v}{\partial y}, \quad (1)$$

where ρ_I is the injection-fluid density; t is the injection time; and R is the casing radius. v_I and v are velocities of the injection-fluid flows into the fracture from wellbore perforation and the fluid velocity in the wellbore, respectively. γ is the pipe open ratio. When generating wellbore grids, the location where there is an existing fracture is taken as one grid, and for this grid, $\gamma = 1$, whereas for other grids, $\gamma = 0$.

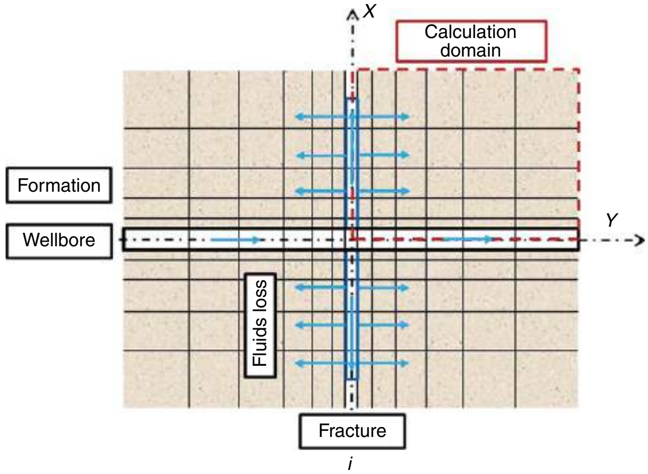

Fig. 2—Top view of flow directions during fracture propagation.

The fracture is assumed to have uniform width and height and is propagating in the x-direction (Fig. 2). In addition, we assume that the fracture has an infinite conductivity at the beginning of creation when injecting water-based fracturing fluid. We use the average fluid-loss velocity depending on both time and position, which is defined by Schechter (1992), to calculate leakoff volume per unit time. The mass balance of fracture propagation is expressed as

$$2wh\frac{\mathrm{d}X_f}{\mathrm{d}t} = whv_x(x,t) - 2h\int_0^{2X_f(t)} \frac{C_{lk}(t)}{\sqrt{t-\tau(x)}}\mathrm{d}x, \quad (2)$$

where w and h are fracture width and height, respectively; X_f is fracture half-length; and v_x is the injection-fluid velocity inside fracture. $v_x = v_I$ at perforation locations where $\gamma = 1$. $C_{lk}(t)$ is the overall leakoff coefficient that considers fluid compressibility, viscosity, and wall-building effects. $\tau(x)$ is the time that the fracture takes to propagate to distance x, after which leakoff starts.

The distance that fluid loss travels into the reservoir from fracture faces can be calculated by integrating the leakoff velocity with respect to leakoff time at specific locations:

$$Y_{lk}(x) = \int_{\tau(x)}^{t} v_{lk}\mathrm{d}t = \int_{\tau(x)}^{t} \frac{C_{lk}}{\sqrt{t-\tau(x)}}\mathrm{d}t, \quad (3)$$

where $Y_{lk}(x)$ is the distance the fluid-loss front travels to the formation, and v_{lk} is the leakoff velocity.

The flow models are solved numerically to account for time-dependent fluid loss. Initially, a no-flow condition is assumed. At perforation locations, wellbore- and fracture-flow models are coupled by the calculated velocity. It should be noted that fractures within the same stage are propagating simultaneously once the injection starts. Fractures in different stages propagate consecutively one stage at a time, and there may be shut-in time between stages. Once a stage is finished with pumping, the stage is simulated as a warm-back stage.

Energy-Conservation Equations. The energy balance in the wellbore to simulate transient temperature profiles is described as

$$\rho_l\hat{C}_{pl}\frac{\partial T}{\partial t} = \frac{2\gamma}{R}\rho_l\hat{C}_{pl}v_I(T_I - T) + \frac{2(1-\gamma)}{R}U_T(T_r - T) - \rho_l\hat{C}_{pl}v\frac{\partial T}{\partial y} - \rho_l vg\sin\theta, \quad (4)$$

where $\hat{C}_{pl}$ is the fluid heat capacity per unit volume and U_T is the overall heat-transfer coefficient between reservoir and wellbore fluid. T is the wellbore temperature; T_I and T_r represent the fracture and reservoir temperature and are calculated by the fracture and the reservoir thermal model, respectively. The left-hand side of Eq. 4 is heat accumulation over a timestep. The first term on the right-hand side is the convective-heat transfer between the wellbore and fracture; the second term represents the heat conduction between the reservoir and wellbore; the third term is heat convection along the well direction; and the last term is the potential term.

The energy-conservation equation in the fracture is expressed as

$$\rho_l\hat{C}_{pl}\frac{\partial T_I}{\partial t} = -\frac{\rho_l\hat{C}_{pl}v_x\partial T_I}{\partial x} - \frac{2\rho_l\hat{C}_{pl}v_{lk}T_I}{w} + \frac{2h_I(T_r - T_I)}{w}, \quad (5)$$

where h_I is the heat-transfer coefficient across fracture faces (Zhao and Tso 1993). Eq. 5 illustrates that energy accumulation of a differential volume in the fracture over time t is the summation of the heat convection caused by fracturing-fluid flow, the convective energy caused by fluid loss, and the heat transfer between the fracturing fluid and surrounding formation.

The transient reservoir thermal model is derived from the general energy-balance equation, and at local position, it is shown as

$$\overline{\rho\hat{C}_p}\frac{\partial T_r}{\partial t} - \phi\beta T_r\frac{\partial p}{\partial t} = -\rho_l\hat{C}_{pl}v_{lk}\frac{\partial T_r}{\partial y} + (\beta T_r - 1)v_{lk}\frac{\partial p}{\partial y} + \frac{\partial}{\partial x}\left(K_e\frac{\partial T_r}{\partial x}\right) + \frac{\partial}{\partial y}\left(K_e\frac{\partial T_r}{\partial y}\right), \quad (6)$$

where $\overline{\rho\hat{C}_p}$ and K_e are the average effective property and average effective reservoir thermal conductivity, respectively, and account for formation fluid and rock; ϕ is the reservoir porosity; and β is the thermal expansion coefficient and can be neglected for water-based

injection fluid. T_r represents the reservoir temperature. The first term on the left-hand side of Eq. 6 is energy accumulation in a differential volume over time t, and the second term represents the transient reservoir-fluid expansion. The first term on the right-hand side is heat convection caused by fluid leakoff into the formation; the second term is the leakoff-fluid expansion; and the third and fourth terms are the heat conductions in the 2D flow system. One should know that the reservoir average effective heat capacity and effective thermal conductivity are not constant for the gridblocks invaded by the fracturing fluid.

Thermal-Model Coupling. To solve for mass- and energy-conservation equations, the fully implicit finite-difference approach is used. Particularly, to efficiently solve the coupled thermal model, the discretization of the wellbore, reservoir, and fracture model is considered conjointly. Initially, the system has a temperature equal to the initial reservoir geothermal temperature everywhere, and proper boundary conditions have to be used for injection and shut-in periods. At the outer boundaries of the calculation domain, where, $x \to \infty$ or $y \to \infty$, a "no heat transfer" condition is applied at all times. Because of the symmetrical problem, at $x = 0$ or $y = 0$, we also have "no heat transfer" boundary conditions at all times. During the injection process, the fracture inner boundary is defined by the wellbore model, and during shut-in period, it is automatically changed to a "no heat transfer" boundary. Moreover, at the fracture/reservoir and wellbore/reservoir interfaces, we use the following boundary conditions ($B.C.s$) to couple thermal models:

$$B.C.s \quad \begin{cases} K_e \dfrac{\partial T_r}{\partial y} = h_l(T_r - T_l), & \text{at } y = y_{\mathrm{res}/fr},\ t \\ K_e \dfrac{\partial T_r}{\partial x} = U_T(T_r - T), & \text{at } x = x_{\mathrm{res}/wb},\ t \end{cases} \qquad (7)$$

Solution Procedure of the Integrated Forward Model

To solve the forward model to simulate temperature distribution along the wellbore with respect to time, we have to couple these models and solve them simultaneously with integration of boundary conditions. The solution procedure of the integrated forward model for single-stage fracturing treatment is presented in **Fig. 3.** Fig. 3 shows that at each timestep for single-stage fracturing, the forward model solves the wellbore-flow model first to obtain fracturing-fluid velocity at perforation locations. When there is a fracture, the model continues to solve the fracture-flow model to obtain the fracture half-length and the injection-fluid velocity inside the fracture, as well as fluid loss into the reservoir. Then, the wellbore, fracture, and reservoir thermal model are solved simultaneously. After the injection time has been ceased, the forward model switches to the shut-in period. There is no fluid flow during shut-in, thus, the invaded reservoir region, the fracture, and the wellbore are warmed up by the geothermal formation. The fluid distribution and temperature profile at the end of injection are used for beginning the shut-in.

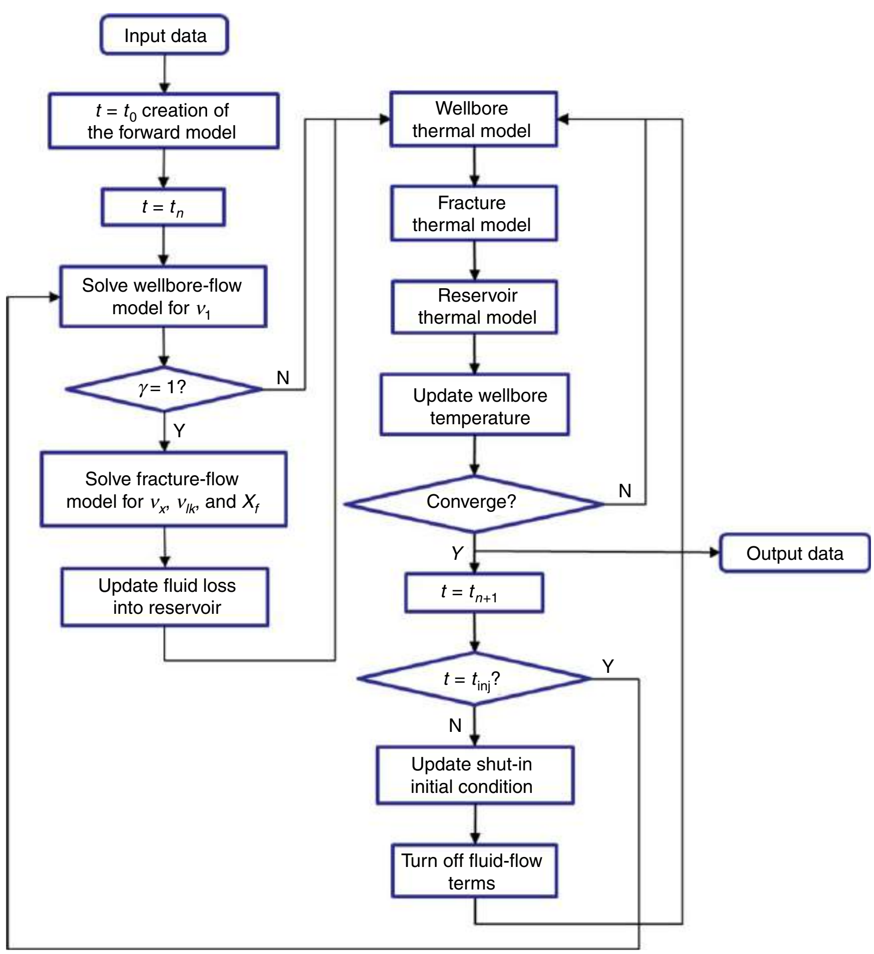

Fig. 3—Solution procedure of single-stage fracturing treatment by use of the integrated forward model.

For multistage fracturing treatments in a horizontal well, real-time control is considered in the wellbore model. Because of the zonal isolation between each stage, the wellbore can be divided into multiple segments according to the stage locations. On the basis of the treatment schedule, the coupled model is called for each segment for either injection or shut-in, respectively. A sequential simulation method is performed to calculate temperature distribution for each segment from toe to heel in the well. At the fracturing stage, all downstream stages have a cold source because of injection, and are warming up by the reservoir after shut-in. All the upstream stages have injection temperature as wellbore temperature. A multistage-fracturing-solution procedure is shown in **Fig. 4.**

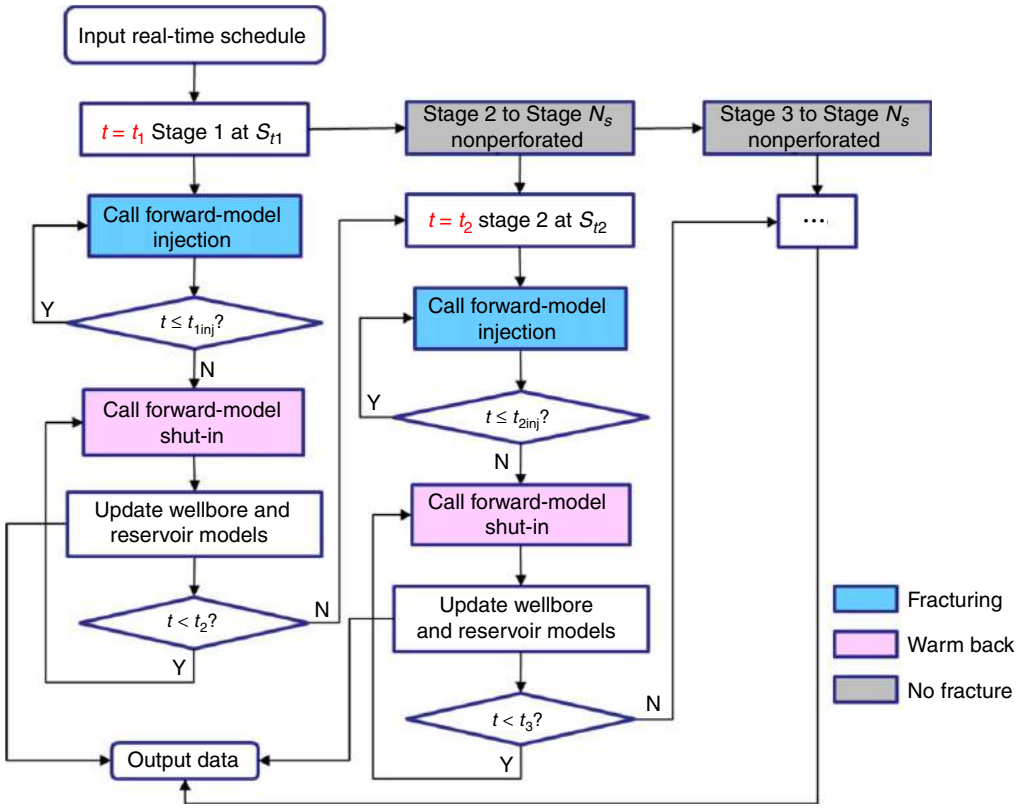

Fig. 4—Solution procedure of multistage fracturing treatments by use of the integrated forward model.

Forward-Model Validation

An analytical solution is available to solve for fracture temperature during injection when assuming there is no fluid loss, and a constant reservoir temperature boundary is used (Wheeler 1969). Similarly, we can use the Green-function solution to solve for conduction-heat transfer in the reservoir during shut-in without fluid-loss convection and given the initial temperature distribution from the end of injection.

We compared the temperature calculated by the developed fracture model with the analytical solution for a hypothetical case. To have the same fracture geometry, we assigned a constant value for fracture-half-length incremental. The fracture and treatment parameters are listed in **Table 1. Table 2** contains the fluid and reservoir properties used in the numerical simulation and analytical calculation.

Fracture and Treatment Parameter	Value	Unit
Injection time, t_{inj}	51.4	min
Injection rate, q_{inj}	22.8	bbl/min
Fracture width, w	0.02	ft
Fracture height, h	160	ft
Fracture half-length, X_f	1,029	ft
Fracture half-length incremental size, Δx	13.8	ft

Table 1—Fracture and treatment parameters for model comparison with analytical solutions.

The temperature comparison of the developed numerical model and analytical model are shown in **Figs. 5 and 6** for fracture and reservoir, respectively. The model is validated by well-matched results with the analytical solutions.

Examples

A synthetic case study is presented to illustrate the application of the integrated forward model on transient temperature analysis. The coupled model is first applied to the single-fracture system to estimate fracture propagation and corresponding temperature behavior. Then, the single-stage fracture treatment with multiple fractures is investigated. Finally, an example of multistage fracturing treatment with multiple fractures per stage is presented. In all examples, the injection rate and time are defined in Table 2..

Reservoir and Fluid Property	Value	Unit
Reservoir initial temperature, T_i	238	°F
Fracturing-fluid-injection temperature (heel), T_{inj}	80	°F
Reservoir porosity, ϕ	0.08	–
Reservoir-rock density, ρ_r	148.6	lbm/ft^3
Fracturing-fluid density, ρ_l	61.6	lbm/ft^3
Reservoir-rock thermal conductivity, K_r	0.000257	Btu/(ft-s-°F)
Reservoir-fluid thermal conductivity, K_f	0.000106	Btu/(ft-s-°F)
Fracturing-fluid thermal conductivity, K_l	0.000106	Btu/(ft-s-°F)
Reservoir-rock heat capacity, C_{pr}	0.2016	Btu/(lbm-°F)
Reservoir-fluid heat capacity, C_{pf}	0.9878	Btu/(lbm-°F)
Fracturing-fluid heat capacity, C_{pl}	0.9878	Btu/(lbm-°F)
Heat-transfer coefficient, h_l	0.002867	Btu/(ft^2-s-°F)

Table 2—Reservoir and fluid properties for model comparison with analytical solutions.

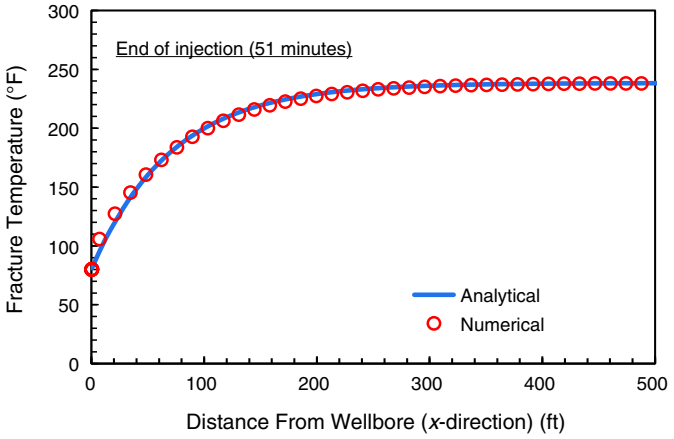

Fig. 5—Fracture temperature comparison with the analytical solution at the end of injection.

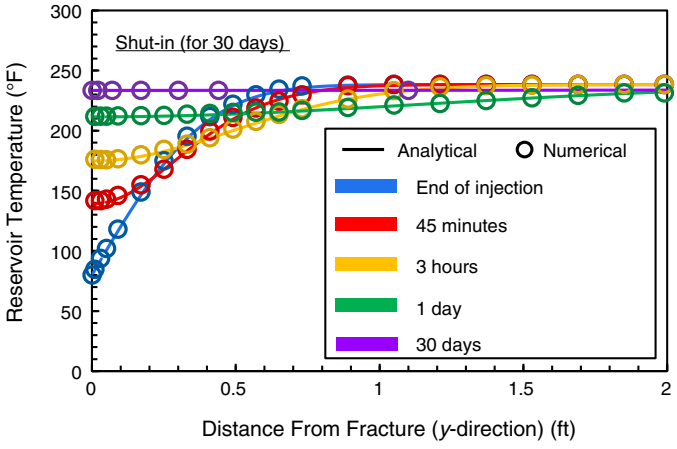

Fig. 6—Reservoir-temperature comparison with the analytical solution from the end of injection to shut-in for 30 days.

Single-Stage Fracture Propagation and Temperature Distribution. The fully coupled model is applied to a single traverse fracture in a horizontal well to investigate fracture propagation, fluid loss, and temperature profile in the fracture and reservoir. Typical shale-gas-reservoir properties are used to create the forward model. The treatment, reservoir, fluid, and well parameters are given in Table 2 for the base case.

Fig. 7 shows the simulated fracture half-length as a function of injection time (Fig. 7a) and the leakoff front at three different injection times (Fig. 7b). The results show that at the end of the injection, the fracture is extended to approximately 600 ft, and the leakoff front with the assumed permeability is approximately only 1.7 in. into the formation at the end of the injection along the horizontal well. As illustrated in Fig. 7b, the near-wellbore region has the most leakoff accumulation, and it contributes to the cooling effect near the wellbore during the injection period. In reality, the reservoir permeability may change during fracturing, and the fracture may also connect with natural fractures; both would result in a much-larger leakoff rate. Such scenarios are studied in the sensitivity analysis.

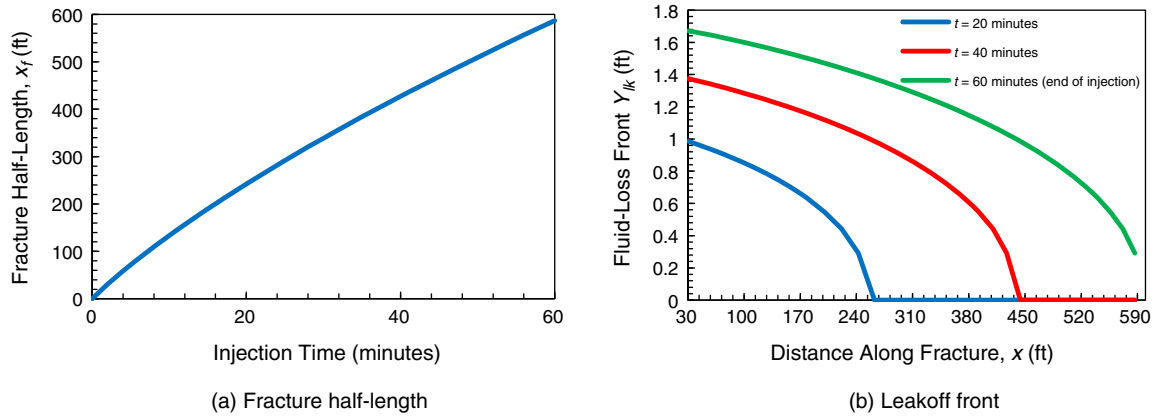

(a) Fracture half-length

(b) Leakoff front

Fig. 7—Fracture half-length and distance of fluid-loss front into the reservoir along the fracture at different times during injection. (a) Fracture half-length; (b) leakoff front.

Fig. 8 displays the temperature contour in 2D (along the wellbore and into the fracture) as a function of injection time. Fig. 8a is at the middle of injection; Fig. 8b is at the end of injection; and Figs. 8c and 8d are the temperature profiles after shut-in at 1 and 5 hours, respectively. During injection, temperature cools off at the fracture location, as expected. Even though the distance of temperature alternation from the fracture along the wellbore is very small, this cooling effect by leakoff changes the temperature behavior at warm back during shut-in time. It is also a clear indication of fracture location. After shut-in, the temperature starts to recover from the cooling of the fracture fluid, and the cooling signal is diminishing as a function of shut-in time. The rate of temperature recovery is a function of how much of the cold fluid is injected at the location.

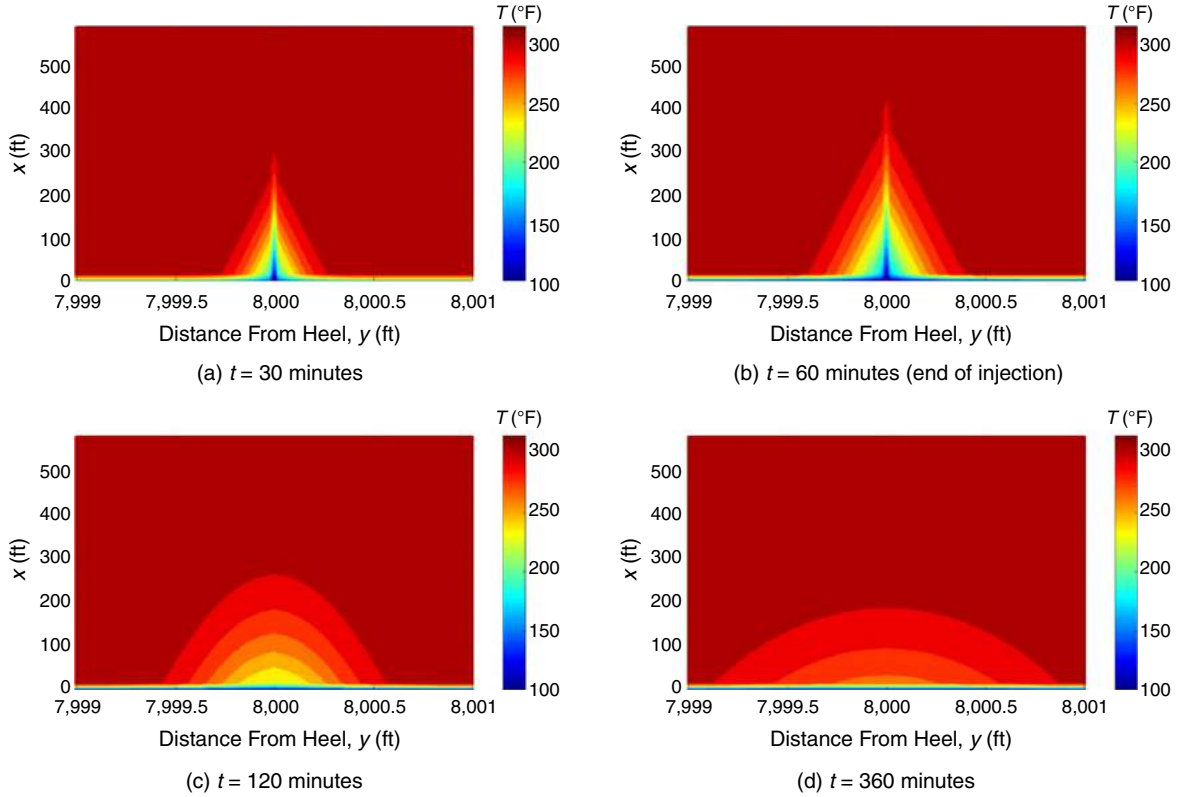

(a) t = 30 minutes

(b) t = 60 minutes (end of injection)

(c) t = 120 minutes

(d) t = 360 minutes

Fig. 8—Temperature map of the single-fracture system during fracturing treatment at various time steps: (a, b) during injection; (c, d) for shut-in at 1 and 5 hours, respectively. (a) t = 30 minutes; (b) t = 60 minutes (end of injection); (c) t = 120 minutes; and (d) t = 360 minutes.

Temperature Response of Single Stage With Multiple Clusters. To investigate the effect of volume of fluid on temperature behavior, we compared the simulated temperature profile if we distribute the total injection volume into two equal fractures instead of one, and the information for this investigation is listed in **Table 3.** The simulated temperature result is displayed in **Fig. 9.** Under the ideal condition, the temperature responds distinctly for one large fracture or two smaller fractures. The cooling locations are clear indications of the locations of created fractures. This feature can be used to determine the number of fractures that are created and to allocate treatment volumes by perforation clusters in one stage. The cooling depth into the reservoir both along the fracture and perpendicular to the fracture is different for the one-fracture case compared with the two-fracture case. The temperature behavior does provide useful information after shut-in for the fracture. Large fractures with deeper cooling recover slower than smaller fractures.

Injection Rate (bbl/min)	Cluster No.	Fracture Spacing (ft)	Fracture Half-Length (ft)
30	1	0	880
30	2	40	440

Table 3—Number of clusters and corresponding fracture half-length at the same total injection rate.

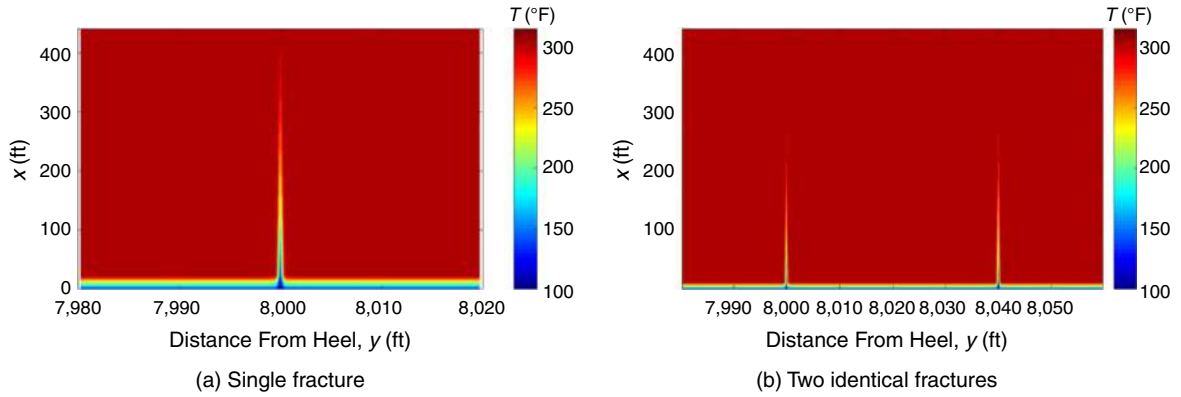

Fig. 9—Temperature map of a single fracture and two identical fractures at the end of injection for the same total injection volume. (a) Single fracture; (b) two identical fractures.

Multistage Multicluster Temperature Profiles. A synthetic case of five stages with five fractures per stage is presented in this example. We assume that the temperature is measured outside the casing, simulating a case of plug-and-perforate completion. The stage length is 200 ft and contains five evenly distributed fractures. In other words, the fracture spacing is 40 ft. For each stage, we inject fracturing fluid for 1 hour and shut-in for 5 hours between stages. Additional information regarding the injection-fluid distribution at each cluster in the example is listed in **Table 4.** For the five stages, fracture half-length is calculated from the injection rate of each stage, which is assigned randomly. **Fig. 10** illustrates the fracture setting used in this example. **Fig. 11** plots the corresponding casing-temperature profiles over time.

Stage 1 at 40 bbl/min					
Cluster No.	1	2	3	4	5
Injection rate (bbl/min)	9	9	8	7	7
Fracture half-length (ft)	264	264	235	205	205
Stage 2 at 60 bbl/min					
Cluster No.	1	2	3	4	5
Injection rate (bbl/min)	10	11	12	12	15
Fracture half-length (ft)	293	323	352	352	440
Stage 3 at 60 bbl/min					
Cluster No.	1	2	3	4	5
Injection rate (bbl/min)	8	10	12	15	15
Fracture half-length (ft)	235	293	352	440	440
Stage 4 at 70 bbl/min					
Cluster No.	1	2	3	4	5
Injection rate (bbl/min)	18	15	12	10	15
Fracture half-length (ft)	528	440	352	293	440
Stage 5 at 50 bbl/min					
Cluster No.	1	2	3	4	5
Injection rate (bbl/min)	10	12	9	10	9
Fracture half-length (ft)	293	352	264	293	264

Table 4—Injection rate and fracture half-length at each cluster for all five stages.

From Fig. 11, we see that the casing-temperature response is complicated and affected by not only the time lag because of zonal isolation, but also the fluid distribution. Therefore, interpretation of field DTS measured data by use of this forward model is a great challenge, and all parameters, both formation properties and treatment design, need to be taken into consideration during the entire fracturing treatment. Sensitivity studies of such important parameters are presented in the following section.

Sensitivity Analysis

The effects of injection rate, leakoff coefficient, and reservoir thermal conductivity on temperature behavior are examined. For each case, a single-stage treatment with five equal fractures is created simultaneously. The fracture spacing is 40 ft and the single-stage

injection time is 1 hour. To examine the effects of DTS cable locations and zonal isolation, the last example considers a single-fracture system and five-stage treatment with a single fracture per stage, respectively. General input parameters are the same as listed in **Tables 5 and 6,** unless redefined specifically.

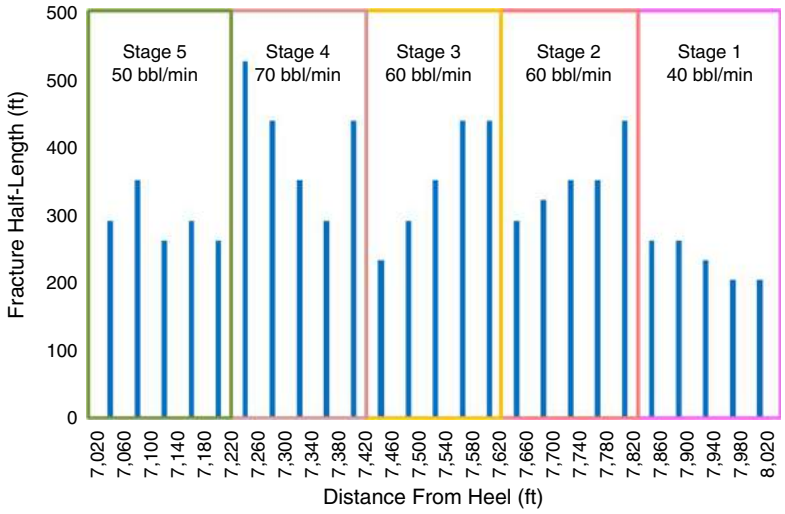

Fig. 10—Fracture half-length of nonuniform fluid distribution for multistage multicluster treatments.

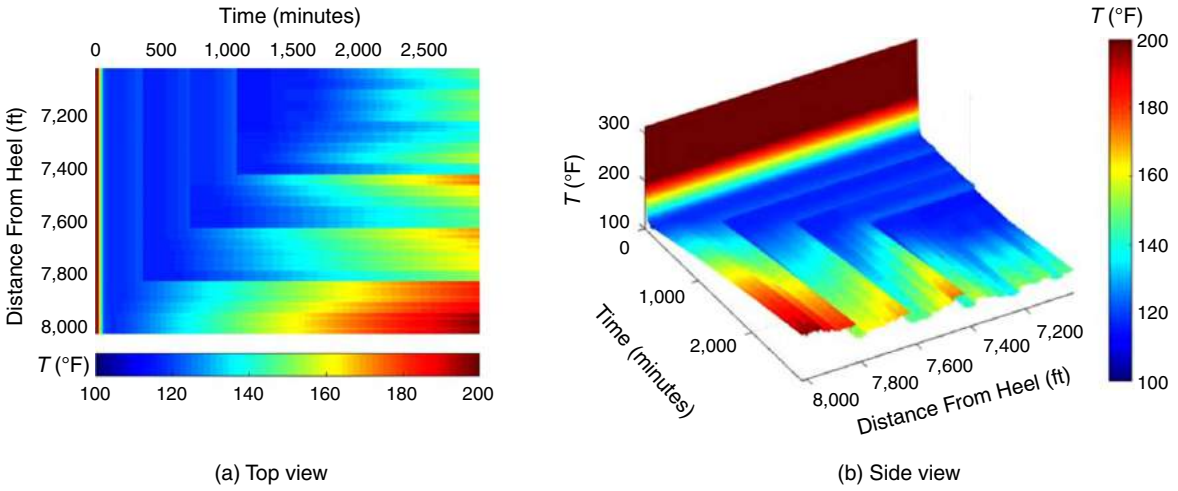

(a) Top view

(b) Side view

Fig. 11—Simulated casing-temperature profiles over time for five-stage fracturing treatments with five nonidentical fractures per stage. (a) Top view; (b) side view.

Treatment and Well Parameter	Value	Unit
Injection time, t_{inj}	60	min
Injection rate, q_{inj}	20	bbl/min
Horizontal-well length, L	8,500	ft
Fracture width, w	0.02	ft
Fracture height, h	150	ft
Hole inner diameter, R_o	8.75	in
Casing outer diameter, R_{ocs}	5.5	in
Casing inner diameter, R_{cs}	4.5	in
Simulation time step, Δt	2	min

Table 5—Treatment and well parameters for synthetic case studies.

Sensitivity to Injection Rate. The effect of injection rate on temperature response is studied with three injection rates. As mentioned previously, there are five fractures created simultaneously in one stage. **Table 7** lists the injection-rate values and corresponding fracture half-length for each case. **Fig. 12** shows the temperature measured at the casing as a function of time at different injection rates

Reservoir, Fluid, and Well Property	Value	Unit
Reservoir initial temperature, T_i	315	°F
Fracturing-fluid-injection temperature (heel), T_{inj}	100	°F
Reservoir porosity, ϕ	0.045	–
Reservoir-rock density, ρ_r	148.6	lbm/ft^3
Reservoir-fluid density, ρ_f	26.2	lbm/ft^3
Fracturing-fluid density, ρ_l	62	lbm/ft^3
Casing density, ρ_{cs}	484	lbm/ft^3
Cement density, ρ_{cm}	196.6	lbm/ft^3
Reservoir-rock thermal conductivity, K_r	0.000257	Btu/(ft-s-°F)
Reservoir-fluid thermal conductivity, K_f	0.000109	Btu/(ft-s-°F)
Fracturing-fluid thermal conductivity, K_l	0.000149	Btu/(ft-s-°F)
Casing thermal conductivity, K_{cs}	0.0016	Btu/(ft-s-°F)
Cement thermal conductivity, K_{cm}	0.000581	Btu/(ft-s-°F)
Reservoir-rock heat capacity, C_{pr}	0.202	Btu/(lbm-°F)
Reservoir-fluid heat capacity, C_{pf}	0.998	Btu/(lbm-°F)
Fracturing-fluid heat capacity, C_{pl}	0.998	Btu/(lbm-°F)
Casing heat capacity, C_{pcs}	0.117	Btu/(lbm-°F)
Cement heat capacity, C_{pcm}	0.22	Btu/(lbm-°F)
Total average leak-off coefficient, C_{lk}	0.0001	ft/√s

Table 6—Reservoir, fluid, and well properties for synthetic case studies.

Injection Rate (bbl/min)	Fracture Half-Length (ft)	*T* at Fracture Locations After Shut-In (°F)
40	234	151.7
60	352	138.8
90	528	129.6

Table 7—Fracture half-length and simulated temperature (after shut-in for 1 day) for five identical fractures.

(Figs. 12a, 12b, and 12c), and the comparison for these injection rates after shut-in for 1 day is shown in Fig. 12d. As illustrated in Fig. 12, lower-temperature response is observed at the fractured locations during injection. Once the injection starts, casing is quickly cooled down by the injection fluid. Similarly, after shut-in of the well, the casing begins to be warmed up by the reservoir. For higher injection rate, the cooling temperature front travels faster into the reservoir and the warm back is slower. Table 7 lists the simulated casing-temperature results after shut-in for 1 day. There are three cases for the same injection time with different injection rates, and we see quantitatively how much the injection volume affects the temperature outside of casing. With higher injection rate, more cold fluid enters the fracture during injection, resulting in a much-slower recovery on temperature during warm back after shut-in. The casing temperature at fracture locations has a 20°F difference when the injection rate increased from 40 bbl/min to 90 bbl/min.

Sensitivity to Fluid Loss. Fluid loss plays an important role in fracturing treatment, which affects the fracture geometry and near-wellbore fluid distribution. The leakoff amount may vary under different circumstances. When there are natural fractures in the reservoir and the hydraulic fracture intercepts the natural fractures, fluid loss can increase dramatically, which can be simulated by use of higher value of leakoff coefficient. To investigate the effect of leakoff amount on fracture propagation and temperature behavior of such scenarios, various leakoff coefficients are considered, and the simulated results are compared. The leakoff coefficients used in the study are 0.0001 ft/$\sqrt{s}$ (base case), and four times higher (0.0004 ft/$\sqrt{s}$) than the base case. The results are shown in **Figs. 13 and 14.**

In Fig. 13a, fracture half-length is displayed for different values of leakoff coefficient for a single fracture. By increasing the leakoff coefficient to four times higher, we see the obvious changes in fracture half-length. Fig. 13b shows the leakoff front into the formation. As leakoff coefficient increases, the leakoff fluid travels much farther into the formation at near-wellbore region. Fig. 14 shows the temperature-simulation result in the reservoir at 1 hour after shut-in for various leakoff coefficients. We find that with larger leakoff coefficient, the temperature map shows less sharpness and the heat flux is more dispersed at the near-wellbore region. Warm back is slower for higher leakoff coefficient.

Sensitivity to Reservoir Thermal Conductivity. For different types of unconventional reservoirs, thermal conductivity may vary in a limited range. However, temperature profile is very sensitive to the reservoir thermal conductivity because of the dominant role of heat conduction during shut-in. To investigate the effect of reservoir thermal conductivity on temperature behavior during fracturing treatment, three different thermal-conductivity values are used here. In the base case, K_r is set to 0.000257 Btu/ft-s-°F, and we also examined the cases for two-times-higher and four-times-higher coefficient. The values used and the simulated casing temperature for these cases after 1 day of shut-in are listed in **Table 8.**

Fig. 15 plots the temperature map of the single fracture system after 1 hour of shut-in for different reservoir-rock thermal conductivities. During the shut-in period, heat conduction is the dominant term. Warm back is much faster when using higher rock thermal conductivity **(Fig. 16).** Simulated casing-temperature profiles over time for multiple reservoir thermal conductivities are also presented for five identical fractures at 40 bbl/min per stage. The same observation was obtained as for the single-fracture case. The casing

temperature recovers from injection cooling during shut-in, and higher reservoir rock thermal conductivity results in quicker recovery (Figs. 16a through 16c). The temperature increases approximately 30°F after 1 day of shut-in when the reservoir rock thermal conductivity is two times higher than the base case (Fig. 16d). We notice that the temperature difference between two-times higher and four-times higher than the base case is smaller.

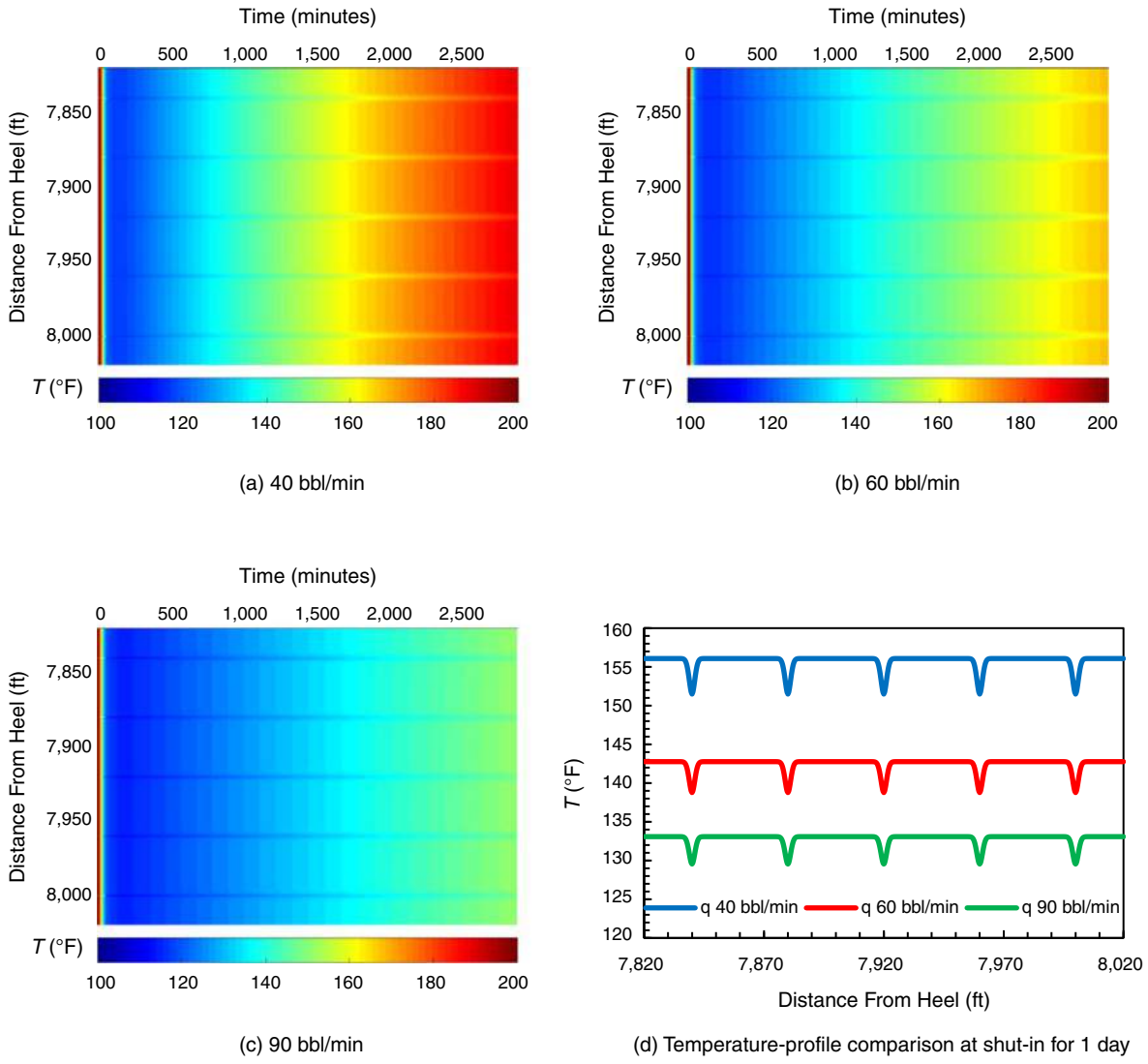

Fig. 12—Simulated casing-temperature profiles for different injection rates and casing-temperature-profile comparison. (a) 40 bbl/min; (b) 60 bbl/min; (c) 90 bbl/min; (d) temperature-profile comparison at shut-in for 1 day.

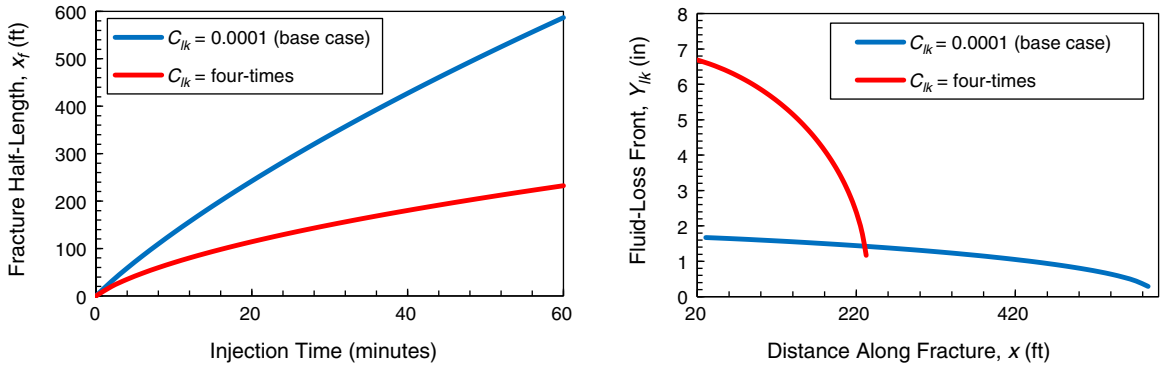

Fig. 13—Fracture half-length and distance the leakoff front travels into the reservoir for various leakoff coefficients during injection. (a) Fracture half-length at different leakoff coefficients; (b) leakoff front into the reservoir.

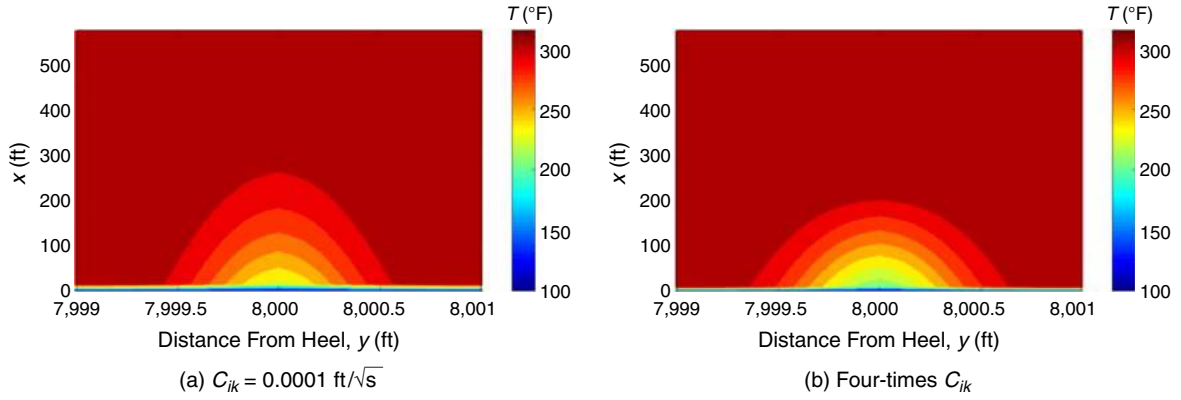

Fig. 14—Temperature maps of the single-fracture system for various leakoff coefficients at 1 hour after shut-in. (a) C_{lk}=0.0001 ft/√s; (b) four-times C_{lk}.

Cases	Rock Thermal Conductivity, K_r [Btu/(ft-s-°F)]	T at Fracture After Shut-In of 1 Day (°F)
Base case	0.000257	151.7
2 times	0.000514	180.5
4 times	0.001028	185.5

Table 8—Rock thermal conductivities and simulated temperature (after 1 day of shut-in).

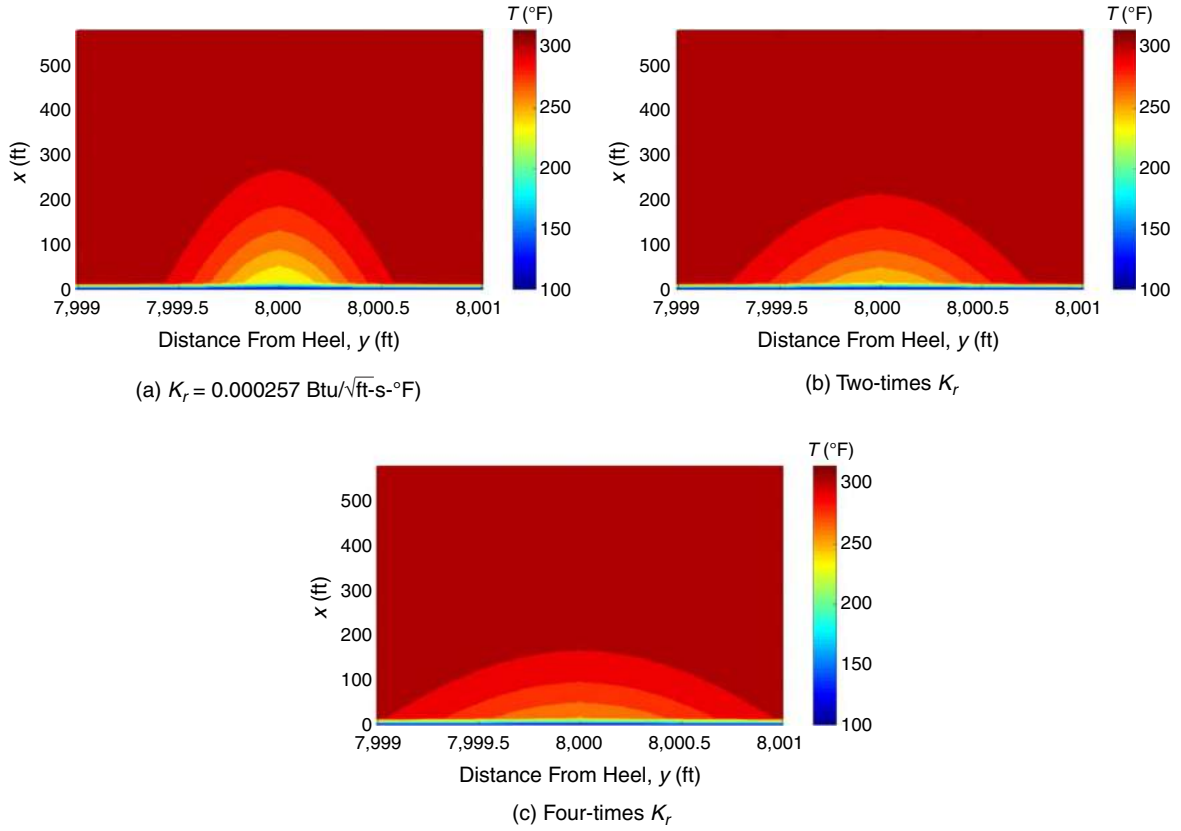

Fig. 15—Temperature maps of the single-fracture system for various reservoir-rock thermal conductivities at shut-in for 1 hour. (a)K_r=0.000257 Btu/(ft-s-°F); (b) two-times K_r; (c) four-times K_r.

Sensitivity to DTS-Deployment Locations. Sierra et al. (2008) stated that the location of the DTS sensor cable has a major effect on temperature response, depending on the thermal conductivity between the fiber cable and the injected-fluid path. For example, DTS cables can be conveyed with coiled tubing inside the wellbore or cemented behind the casing. The integrated model is able to simulate the temperature profile at DTS measured locations for different DTS cable-coupling scenarios. To examine the temperature difference because of sensor locations, we simulated temperature history inside the wellbore and outside the casing for a single-fracture system by use of the same case defined by Tables 5 and 6. **Fig. 17** displays the temperature response at the wellbore, casing, and reservoir (the middle of the first reservoir gridblock attached to the wellbore and fracture, 15 ft into the reservoir) locations during the fracturing

treatment. Fig. 17a shows that temperature behaves differently at all three locations during injection, and this results in a different recovery after shut-in. We are more interested in the temperature difference between the locations inside the wellbore and outside the casing (where temperature is measured). Fig. 17b enlarges the temperature scale to focus on the wellbore and casing temperature only. During injection, the wellbore is filled with injection fluid, and it is reasonable to assume that the wellbore temperature is immediately reduced to the injection temperature. The casing temperature is influenced by the heat transfer through the casing and it is directly in contact with the formation rock, and thus the temperature is much higher to start with. At the end of the injection, the temperature is approximately 10°F different between the wellbore and casing. This difference does not last long after shut-in. Temperature merged to the same value after approximately 2 hours of shut-in.

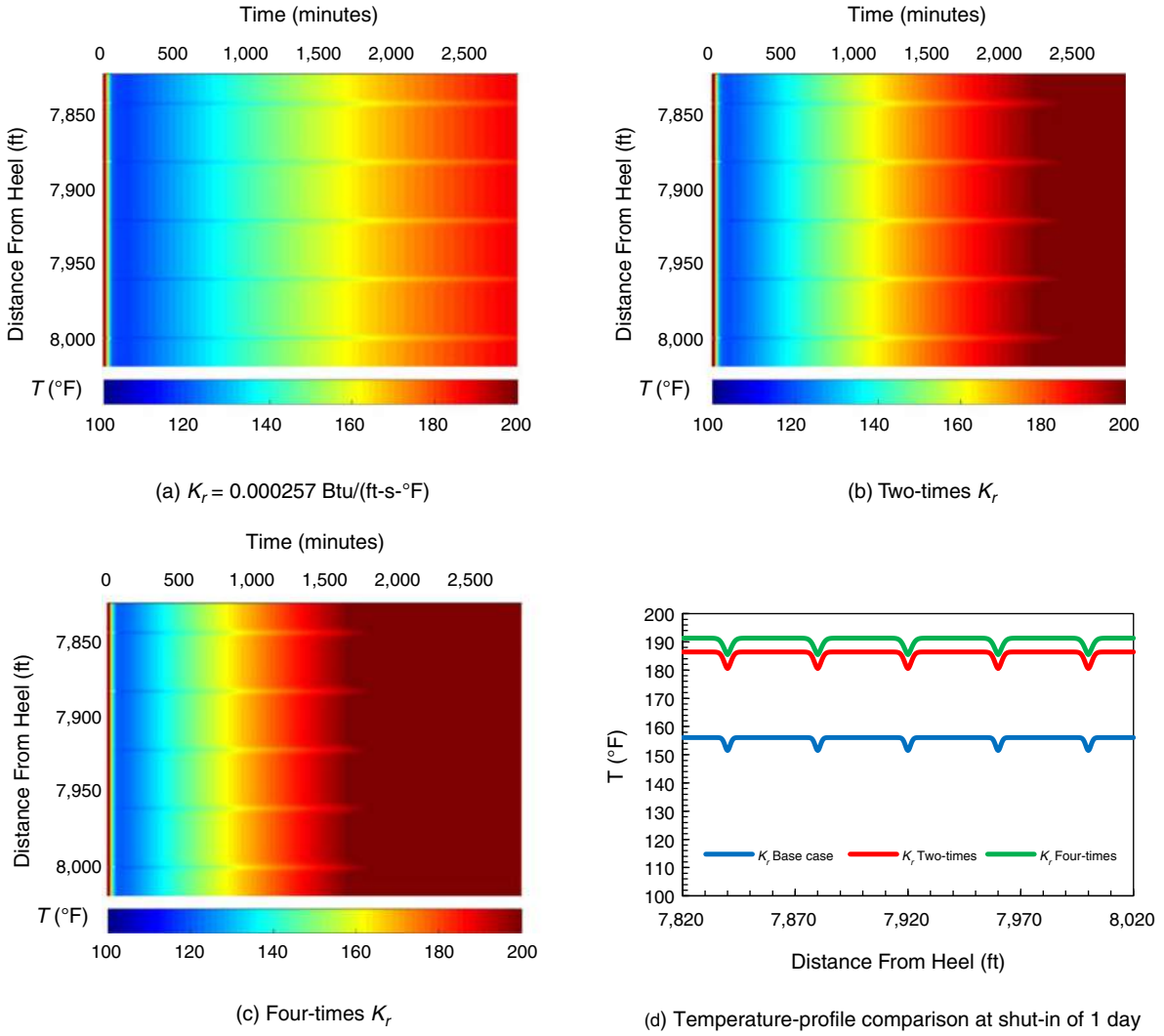

Fig. 16—Simulated casing-temperature profiles over time of single stage with five identical fractures for various reservoir-rock thermal conductivities, and casing-temperature profile for these three rock thermal conductivities after 1 day of shut-in. (a) K_r=0.000257 Btu/(ft-s-°F); (b) two-times K_r; (c) four-times K_r; (d) temperature-profile comparison at shut-in of 1 day.

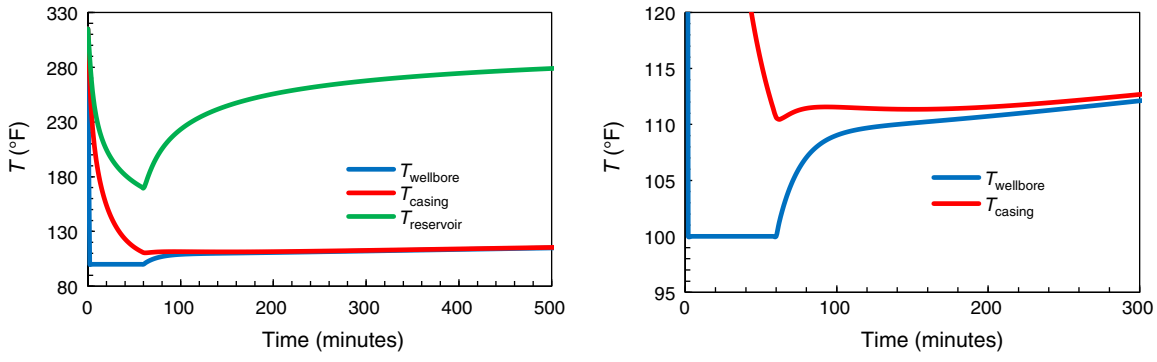

Fig. 17—Simulated temperature profiles for different DTS thermal coupling scenarios for single-fracture system during injection and shut-in. (a) Temperature at wellbore, casing, and reservoir; (b) enlarged wellbore and casing temperature.

For multistage fracturing treatment, stages are isolated. With plug-and-perf completion, the well is shut-in between stages to set the plug to separate the previous stage and prepare for injection of the following stage. A hypothetical case is studied with a sequential treatment schedule, with 1-hr injection for each stage, followed by 5 hours of shut-in. A single fracture per stage is considered to avoid complication. The stage space is 40 ft. The schematic of this five-stage treatment is shown in **Fig. 18.** Simulated wellbore- and casing-temperature profiles over time for five nonidentical stages are presented. The additional input information besides Tables 5 and 6 is listed in **Table 9.**

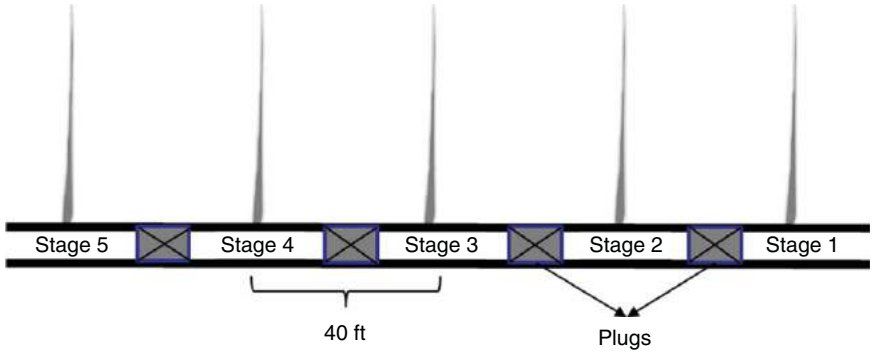

Fig. 18—Schematic of five-stage treatment with single fracture per stage.

Nonidentical Fractures at Five Stages					
Stage No.	1	2	3	4	5
Injection rate (bbl/min)	5	7	10	8	10
Fracture half-length (ft)	147	205	293	235	293

Table 9—Injection rate and fracture half-length at each stage.

Fig. 19a illustrates that during injection, the well shows the injection-fluid temperature as long as we keep injecting cold fluid to propagate fractures. The temperature at fractured locations is lowest. With good isolation, the distinct temperature that changed from one stage to another can be identified. The casing-temperature profiles in this case are shown in Fig. 19b. At the casing location, even without injection-temperature marks, temperature can clearly show the stage transition. This information is valuable when used to diagnose zonal isolation. If there is leakage between the stages, we would not see the clear warm-up behavior at the stage shut-in.

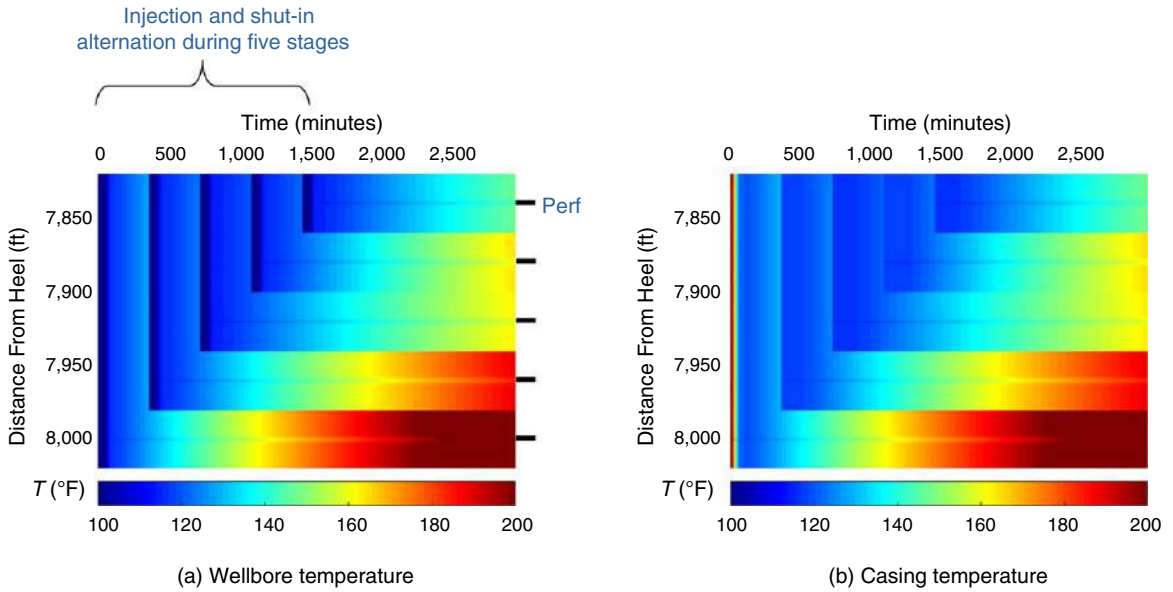

Fig. 19—Simulated wellbore and casing temperature profiles for five nonidentical stages with single fracture per stage. (a) Wellbore temperature; (b) casing temperature.

The developed model can be used as a standalone simulation tool to predict temperature behavior during fracture and after shut-in, or used as an initial condition for temperature monitoring during production. **Fig. 20** shows the ability of the model when used to simulate a 10-stage fracture job with five clusters in each stage. The temperature simulated is up to 1 week of shut-in. The computation time of a case like this is a few hours. After 1 week, we still see lower-temperature signals at fractured locations. This illustrates the potential

of using DTS-measured temperature data to allocate fractures and interpret fluid distribution. Moreover, the integrated forward model can provide initial conditions for thermal and flow modeling of fractured-well production instead of assuming that temperature and fluid are the same as the initial reservoir condition.

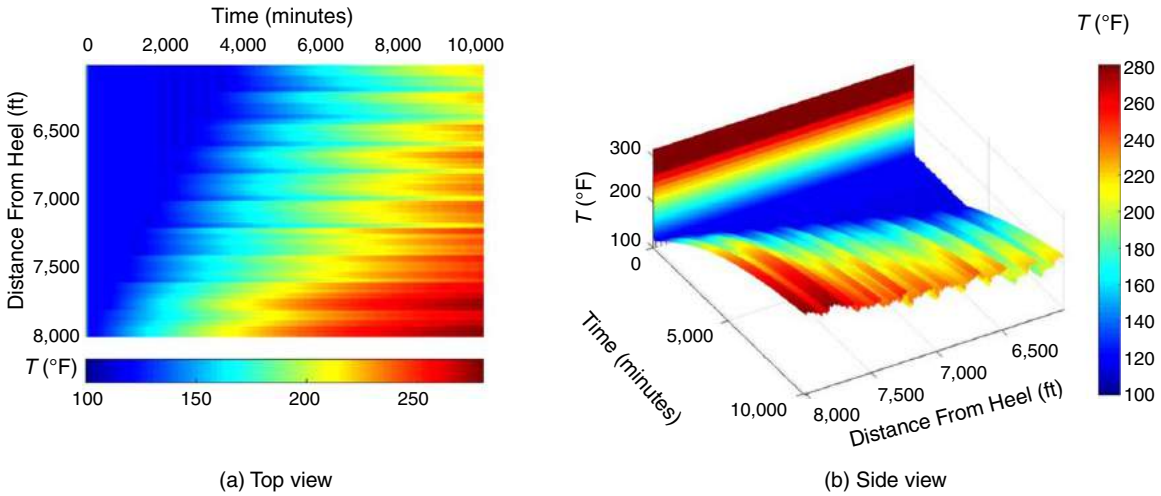

Fig. 20—Simulated casing temperature of 10-stage nonidentical fractures over 1 week. (a) Top view; (b) side view.

Conclusion

In this study, we developed an integrated model to simulate transient temperature behavior in the wellbore, fracture, and reservoir during multistage fracture treatments in horizontal wells. Instantaneous multifracture propagation within the same stage and sequential propagation for multiple stages are considered in the forward model. From synthetic cases and sensitivity studies, we conclude the following:

1. The model simulated temperature behavior during injection and after shut-in for different well completions and fracture procedures. By use of the rigorous theory, the model captures the temperature characteristics as a function of injection volume, reservoir thermal properties, and completion structure.
2. Temperature response is sensitive to injection rate during fracturing. Therefore, measured DTS data can be used to locate fractures and allocate treatment volumes by perforation clusters.
3. Leakoff is important when simulating temperature behavior. Higher leakoff results in wider cold-fluid invasion into the formation but shorter fracture half-length, which affects transient temperature behavior at the near-wellbore region.
4. The DTS-deployment location and zonal isolation affect measured temperature behavior. Temperature data acquired from outside of casing contain lower noise and have no physical interference from wellbore flow, resulting in higher data quality for interpretation.
5. The model can either serve as a standalone tool to diagnose fracture treatment or provide more-accurate initial conditions for thermal and flow modeling of fractured-well production.

Nomenclature

C_{lk} = overall average leakoff coefficient, $LT^{-\frac{1}{2}}$, $ft/\sqrt{s}$
C_{pcm} = cement heat capacity, $L^2T^{-2}K^{-1}$, Btu/(lbm-°F)
C_{pcs} = casing heat capacity, $L^2T^{-2}K^{-1}$, Btu/(lbm-°F)
$\hat{C}_{pf}$ = reservoir-fluid heat capacity per unit volume, $L^2T^{-2}K^{-1}$, Btu/(lbm-°F)
$\hat{C}_{pl}$ = injection-fluid heat capacity per unit volume, $L^2T^{-2}K^{-1}$, Btu/(lbm-°F)
$\hat{C}_{pr}$ = reservoir-rock heat capacity per unit volume, $L^2T^{-2}K^{-1}$, Btu/(lbm-°F)
g = gravitational constant, LT^{-2}, ft/s^2
h = fracture height, L, ft
h_l = Newton's cooling-heat-transfer coefficient, $MT^{-3}K^{-1}$, Btu/(ft^2-s-°F)
K_{cs} = casing thermal conductivity, $MLT^{-3}K^{-1}$, Btu/(ft-s-°F)
K_{cm} = cement thermal conductivity, $MLT^{-3}K^{-1}$, Btu/(ft-s-°F)
K_e = effective thermal conductivity, $MLT^{-3}K^{-1}$, Btu/(ft-s-°F)
K_f = reservoir-fluid thermal conductivity, $MLT^{-3}K^{-1}$, Btu/(ft-s-°F)
K_l = injection-fluid thermal conductivity, $MLT^{-3}K^{-1}$, Btu/(ft-s-°F)
K_r = reservoir-rock thermal conductivity, $MLT^{-3}K^{-1}$, Btu/(ft-s-°F)
L = horizontal well length, L, ft
N_s = stage number, dimensionless
p = pressure, $ML^{-1}T^{-2}$, psi
q_{inj} = injection-flow rate, L^3T^{-1}, bbl/min
R = wellbore diameter, L, in.
R_{cs} = casing inner diameter, L, in.
R_o = hole inner diameter, L, in.
R_{ocs} = casing outer diameter, L, in.
S_t = stage location, L, ft
t = time, T, minutes
T = wellbore temperature, K, °F

T_i = reservoir initial temperature, K, °F
T_{inj} = injection fluid temperature, K, °F
T_l = fracture temperature, K, °F
T_r = reservoir temperature, K, °F
U_T = overall heat-transfer coefficient, $MT^{-3}K^{-1}$, Btu/(ft^2-s-°F)
v = injection-fluid velocity in wellbore, LT^{-1}, ft/sec
v_I = injection-fluid velocity into the fracture at perforation locations, LT^{-1}, ft/sec
v_{lk} = fluid-loss velocity, LT^{-1}, ft/sec
v_x = fluid velocity in x-direction, LT^{-1}, ft/sec
w = average fracture width, L, ft
X_f = fracture half-length, L, ft
Y_{lk} = fluid-loss front, L, ft
β = thermal expansion coefficient, K^{-1}, 1/°F
γ = pipe open ratio, dimensionless
θ = wellbore-inclination angle, radians
ρ_{cm} = cement density, ML^{-3}, lbm/ft^3
ρ_{cs} = casing density, ML^{-3}, lbm/ft^3
ρ_f = reservoir-fluid density, ML^{-3}, lbm/ft^3
ρ_l = injection-fluid density, ML^{-3}, lbm/ft^3
ρ_r = reservoir-rock density, ML^{-3}, lbm/ft^3
$\tau(x)$ = time for fracture to propagate to x, T, minutes
ϕ = reservoir porosity, dimensionless

Subscripts

n = timestep index
res/fr = reservoir/fracture interface
res/wb = reservoir/wellbore interface

References

Amini, K., Soliman, M. Y., and House, W. V. 2015. A Three-Dimensional Thermal Model for Hydraulic Fracturing. Presented at the SPE Annual Technical Conference and Exhibition, Houston, 28–30 September. SPE-174858-MS. https://doi.org/10.2118/174858-MS.

Bahonar, M., Azaiez, J., and Chen, Z. 2010. A Semi-Unsteady-State Wellbore Steam/Water Flow Model for Prediction of Sandface Conditions in Steam Injection Wells. *J Can Pet Technol* **49** (9): 13–21. SPE-140663-PA. https://doi.org/10.2118/140663-PA.

Duru, O. O. and Horne, R. N. 2008. Modeling Reservoir Temperature Transients and Matching to Permanent Downhole Gauge Data for Reservoir Parameter Estimation. Presented at the SPE Annual Technical Conference and Exhibition, Denver, 21–24 September. SPE-115791-MS. https://doi.org/10.2118/115791-MS.

Hagoort, J. 2004. Ramey's Wellbore Heat Transmission Revisited. *SPE J.* **9** (4): 465–474. SPE-87305-PA. https://doi.org/10.2118/87305-PA.

Hasan, A. R. and Kabir, C. S. 1991. Heat Transfer During Two-Phase Flow in Wellbores: Part I–Formation Temperature. Presented at the SPE Annual Technical Conference and Exhibition, Dallas, 6–9 October. SPE-22866-MS. https://doi.org/10.2118/22866-MS.

Hoang, H., Mahadevan, J., and Lopez, H. D. 2011. Interpretation of Wellbore Temperatures Measured Using Distributed Temperature Sensors During Hydraulic Fracture. Presented at the SPE Hydraulic Fracturing Technology Conference, The Woodlands, Texas, 24–26 January. SPE-140442-MS. https://doi.org/10.2118/140442-MS.

Holley, E. H., Molenaar, M. M., Fidan, E. et al. 2012. Interpreting Uncemented Multistage Hydraulic-Fracturing Completion Effectiveness Using Fiber-Optic DTS Injection Data. Presented at the SPE Middle East Unconventional Gas Conference and Exhibition, Abu Dhabi, 23–25 January. SPE-153131-MS. https://doi.org/10.2118/153131-MS.

Huckabee, P. T. 2009. Optic Fiber Distributed Temperature for Fracture Stimulation Diagnostics and Well Performance Evaluation. Presented at the SPE Hydraulic Fracturing Technology Conference, The Woodlands, Texas, 19–21 January. SPE-118831-MS. https://doi.org/10.2118/118831-MS.

Johnson, D. O., Sierra, J. R., Kaura, J. D. et al. 2006. Successful Flow Profiling of Gas Wells Using Distributed Temperature Sensing Data. Presented at the SPE Annual Technical Conference and Exhibition, San Antonio, Texas, 24–27 September. SPE-103097-MS. https://doi.org/10.2118/103097-MS.

Kamphuis, H., Davies, D. R., and Roodhart, L. P. 1993. A New Simulator for the Calculation of the In Situ Temperature Profile During Well Stimulation Fracturing Treatments. *J Can Pet Technol* **32** (5): 38–47. PETSOC-93-05-03. https://doi.org/10.2118/93-05-03.

Li, Z. and Zhu, D. 2010. Predicting Flow Profile of Horizontal Well by Downhole Pressure and Distributed-Temperature Data for Waterdrive Reservoir. *SPE Prod & Oper* **25** (3): 296–304. SPE-124873-PA. https://doi.org/10.2118/124873-PA.

Maubeuge, F., Didek, M. P., Beardsell, M. B. et al. 1994a. Temperature Model for Flow in Porous Media and Wellbore. Presented at the SPWLA 35th Annual Logging Symposium, Tulsa, 19–22 June. SPWLA-1994-N.

Maubeuge, F., Arquis, E., and Bertrand, O. et al. 1994b. MOTHER: A Model for Interpreting Thermometrics. Presented at the SPE Annual Technical Conference and Exhibition, New Orleans, 25–28 September. SPE-28588-MS. https://doi.org/10.2118/28588-MS.

Meyer, B. R. 1989. Heat Transfer in Hydraulic Fracturing. *SPE Res Eng* **4** (4): 423–429. SPE-17041-PA. https://doi.org/10.2118/17041-PA.

Molenaar, M. M., Fidan, E., and Hill, D. J. 2012. Real-Time Downhole Monitoring of Hydraulic Fracturing Treatments Using Fibre Optic Distributed Temperature and Acoustic Sensing. Presented at the SPE/EAGE European Unconventional Resources Conference and Exhibition, Vienna, Austria, 20–22 March. SPE-152981-MS. https://doi.org/10.2118/152981-MS.

Ouyang, L.-B. and Belanger, D. L. 2006. Flow Profiling by Distributed Temperature Sensor (DTS) System–Expectation and Reality. *SPE Prod & Oper* **21** (2): 269–281. SPE-90541-PA. https://doi.org/10.2118/90541-PA.

Ramey, H. J. 1962. Wellbore Heat Transmission. *J Pet Technol* **14** (4): 427–435. SPE-96-PA. https://doi.org/10.2118/96-PA.

Schechter, R. S. 1992. *Oil Well Stimulation*, first edition. Englewood Cliffs, New Jersey: Prentice Hall.

Seth, G., Reynolds, A. C., and Mahadevan, J. 2010. Numerical Model for Interpretation of Distributed-Temperature-Sensor Data During Hydraulic Fracturing. Presented at the SPE Annual Technical Conference and Exhibition, Florence, Italy, 19–22 September 2010. SPE-135603-MS. https://doi.org/10.2118/135603-MS.

Sierra, J. R., Kaura, J. D., Gualtieri, D. et al. 2008. DTS Monitoring Data of Hydraulic Fracturing: Experiences and Lessons Learned. Presented at the SPE Annual Technical Conference and Exhibition, Denver, 21–24 September. SPE-116182-MS. https://doi.org/10.2118/116182-MS.

Sui, W. 2009. *Determining Multilayer Formation Properties from Transient Temperature and Pressure Measurements*. PhD dissertation, Texas A&M University, College Station, Texas (August 2009).

Tabatabaei, M. and Zhu, D. 2011. Fracture Stimulation Diagnostics in Horizontal Wells Using DTS. Presented at the Canadian Unconventional Resources Conference, Calgary, 15–17 November. SPE-148835-MS. https://doi.org/10.2118/148835-MS.

Ugueto, G. A., Ehiwario, M., Grae, A. et al. 2014. Application of Integrated Advanced Diagnostics and Modeling to Improve Hydraulic Fracture Stimulation Analysis and Optimization. Presented at the SPE Hydraulic Fracturing Technology Conference, The Woodlands, Texas, 4–6 February. SPE-168603-MS. https://doi.org/10.2118/168603-MS.

Ugueto, G. A., Huckabee, P. T., and Molenaar, M. M. 2015. Challenging Assumptions About Fracture Stimulation Placement Effectiveness Using Fiber Optic Distributed Sensing Diagnostics: Diversion, Stage Isolation and Overflushing. Presented at the SPE Hydraulic Fracturing Technology Conference, The Woodlands, Texas, 3–5 February. SPE-173348-MS. https://doi.org/10.2118/173348-MS.

Wheeler, J. A. 1969. Analytical Calculations For Heat Transfer From Fractures. Presented at the SPE Improved Oil Recovery Symposium, Tulsa, 13–15 April. SPE-2494-MS. https://doi.org/10.2118/2494-MS.

Yoshioka, K., Zhu, D., Hill, A. D. et al. 2007. Prediction of Temperature Changes Caused by Water or Gas Entry into a Horizontal Well. *SPE Prod & Oper* **22** (4): 425–433. SPE-100209-PA. https://doi.org/10.2118/100209-PA.

Zhao, J. and Tso, C. P. 1993. Heat Transfer by Water Flow in Rock Fractures and the Application to Hot Dry Rock Geothermal Systems. *Int. J. Rock Mech. Min.* **30** (6): 633–641. https://doi.org/10.1016/0148-9062(93)91223-6.

Xinyang Li recently earned a PhD degree from at Texas A&M University. Her research mainly focuses on unconventional reservoirs, hydraulic-fracturing design and diagnostics, horizontal intelligent wells, and geothermal modeling. Li has expertise in the areas of well completion and stimulation, reservoir simulation, reserves and economic evaluations, and multiphase-flow dynamics. She holds a bachelor's degree in oil and gas storage and transportation engineering from China University of Petroleum, and a master's degree in petroleum engineering from the University of Tulsa.

Ding Zhu is a professor in the Petroleum Engineering Department at Texas A&M University. Her research areas are production engineering, well stimulation, intelligent-well modeling, and complex well-performance optimization. Zhu has authored or coauthored more than 160 technical papers, and is coauthor of the textbook *Petroleum Production Systems* (second edition) and the SPE book *Multilateral Wells*. She has been a committee member and chairperson for many SPE conferences and events, and is currently an associate editor for *SPE Production & Operations*. Zhu is an SPE Distinguished Member. She holds a bachelor's degree in mechanical engineering from the University of Science and Technology, Beijing, and master's and PhD degrees in petroleum engineering, both from the University of Texas at Austin.